Available online at www.sciencedirect.com

ScienceDirect

Advances in Space Research 67 (2021) 3504–3514

ADVANCES IN SPACE RESEARCH (a COSPAR publication)

www.elsevier.com/locate/asr

Connectivity preservation and collision avoidance control for spacecraft formation flying in the presence of multiple obstacles

Xianghong Xue *, Xiaokui Yue *, Jianping Yuan

National Key Laboratory of Aerospace Flight Dynamics, Xi'an 710072, PR China
School of Astronautics, Northwestern Polytechnical University, Xi'an 710072, PR China

Received 17 December 2019; received in revised form 14 May 2020; accepted 25 May 2020
Available online 6 June 2020

Abstract

This paper addresses connectivity preservation and collision avoidance problem of spacecraft formation flying with multiple obstacles and parametric uncertainties under a proximity graph. In the proximity graph, each spacecraft can only get the states of the neighbor spacecraft within its sensing region. Connectivity preservation of a graph means that the connectivity of the graph should be preserved at all times during spacecraft formation flying. We consider two cases: (i) the obstacles are static, and (ii) the obstacles are dynamic. In the first case, a distributed continuous control algorithm based on artificial potential function and equivalent certainty principle is proposed to account for the unknown parameters and the static obstacles. In the second case, a sliding surface combined with a distributed adaptive control algorithm is proposed to tackle the influence of the dynamic obstacles and the unknown parameters at the same time. With the distributed control algorithms, the desired formation configuration can be achieved while the connectivity of the graph is preserved and the collisions between the spacecraft and the obstacles are avoided. Numerical simulations are presented to illustrate the theoretical results.

Keywords: Spacecraft formation flying; Connectivity preservation; Obstacle avoidance; Distributed adaptive control

1. Introduction

Spacecraft formation flying (SFF) has received considerable attention due to its apparent advantages, such as flexibility, reliability, robustness and low fuel consumption (Liu and Zhang, 2018). These advantages make SFF a competitive method to implement space missions, including synthetic aperture radars, gravity field measurement, space-based interferometers and distributed satellite architecture (Di Mauro et al., 2017; Bandyopadhyay et al., 2016). One of the critical issues for SFF is to design distributed control algorithms to achieve formation reconfiguration or formation maintenance.

Therefore, each spacecraft acts in a distributed manner to perform the global tasks cooperatively with only local information from its neighbors to increase the flexibility and robustness of SFF. Most current literature assume the communication graph is connected at any time (Zou et al., 2016; Yue et al., 2019). However, the connectivity of the communication network is directly related to the relative distances between the spacecraft, which is constrained by the communication distance between the spacecraft. Therefore, a more practical question is how to preserve the connectivity of the network at all times (Knorn et al., 2016).

The connectivity preservation problem has been widely investigated in multi-agent systems and mobile robotic systems in the past twe decades (Zavlanos and Pappas,

* Corresponding authors at: National Key Laboratory of Aerospace Flight Dynamics, Xi'an 710072, PR China.
E-mail addresses: xhxue@mail.nwpu.edu.cn (X. Xue), xkyue@nwpu.edu.cn (X. Yue), jyuan@nwpu.edu.cn (J. Yuan).

https://doi.org/10.1016/j.asr.2020.05.036
0273-1177/

2007; Qu et al., 2014; Stephan et al., 2017; Deng et al., 2018). The methods to settle this problem can be divided into two categories: the optimization-based methods (Kim and Mesbahi, 2006; De Gennaro and Jadbabaie, 2006) and the artificial potential function (APF) based methods (Ji and Egerstedt, 2007; Cao and Ren, 2012). The positive of algebraic connectivity of a graph (the second smallest eigenvalue of the Laplacian matrix of a graph) is a typical metric to indicate that the graph is connected. The optimization-based method fulfills connectivity preservation by maximizing algebraic connectivity. A optimization-based method using algebraic connectivity is a proposed in (Kim and Mesbahi, 2006). However, this method is centralized and requires the global information about the communication graph. Then, literature (Sabattini et al., 2015) developed this method to a decentralized method by estimating the algebraic connectivity of the graph. The global property of optimization-based method led it can be used to add or delete communication links in a graph. But, the estimation of algebraic connectivity is time-consuming and difficult to meet real-time requirement. Literature (Ji and Egerstedt, 2007) proposed a distributed coordination controller for the connectivity preservation of multi-agent systems by designing appropriate weights of a potential function to different agents. Then, this method was developed to the multi-robot system and performed with a bounded control law in (Gasparri et al., 2017). More information about connectivity preservation control of multi-agent systems can be found in (Zavlanos et al., 2011; Dong and Huang, 2017; Lu, 2018) and reference therein.

Recently, some studies have begun to consider the connectivity preservation control of SFF. Literature (Xue et al., 2019) provided a potential function based control method to avoid the collisions between spacecraft and preserve the connectivity of communication networks in the presence of parameter uncertainties. Literature (Ghapani et al., 2016) employed equivalent certainty principle to design adaptive connectivity preservation control laws for leader–follower Lagrange systems in the presence of parameter uncertainties. The authors presented simulations of SFF with spacecraft relative dynamics to illustrate the effectiveness of the adaptive control laws. However, the above results didn't consider the impact of space obstacles.

Debris in space and other spacecraft might threaten the spacecraft in formation. Therefore, it is necessary to consider the collision avoidances between the spacecraft and the obstacles. Collision avoidance methods for SFF include the behavior-based methods (Balch and Arkin, 1998; Schlanbusch et al., 2011; Zhou et al., 2018) and the APF based methods (Huang et al., 2017; Hu et al., 2015). The null-space based method adopted in (Schlanbusch et al., 2011; Zhou et al., 2018) is a typical behavior-based cooperative formation control method. Artificial potential function is widely used in SFF because it is easy to integrate with the controller design. Literature (Huang et al., 2017) investigated under actuated collision avoidance for spacecraft formation reconfiguration in circular orbits. Reference (Hu et al., 2015) proposed a couple of control laws based on sliding mode and equivalent certainty principle for leader–follower SFF in the presence of obstacle. However, the method is not distributed as the authors assumed that each spacecraft can obtain the states of all spacecraft and the obstacle.

Nevertheless, to the best of the authors' knowledge, few studies consider the connectivity preservation of the communication graph in SFF. Furthermore, the problem of combining obstacle avoidance and connectivity preservation with spacecraft formation reconfiguration poses considerable complexity and difficulty, and it remains an open issue. Obstacle avoidance creates a potential threat to disconnect the communication network due to the repulsive force generated between the spacecraft and the obstacles. Inspired by the previous discussions, we focus on the distributed connectivity preservation and collision avoidance of SFF in the presence of multiple obstacles. Firstly, the communication graph between the spacecraft is constructed dynamically according to the relative distances between all spacecraft. Besides, two artificial potential functions, including formation potential function and obstacle avoidance potential function are presented. Two control laws based on the artificial potential functions and certainty equivalence principle are designed for SFF in the presence of static and dynamic obstacles. Moreover, the sliding mode technique is used to tackle the dynamic obstacles. It is shown that the control laws can preserve the connectivity of the graph and avoid the collisions between the spacecraft and the obstacles.

The paper is organized as follows: Section 2 states the relative dynamics of spacecraft formation system and some notions about algebraic graph theory. The potential functions and controller design are proposed in Section 3. Numerical simulations are presented in Section 4 to demonstrate various features and effectiveness of the proposed control methods. Finally, the paper is completed with some concluding comments in Section 5.

2. Background

In this paper, we mainly study how to preserve the connectivity of the communication graph and avoid collisions between the spacecraft and obstacles during formation reconfiguration. This section provides the relative dynamics of the spacecraft and some notions of algebraic graph theory.

2.1. Spacecraft relative dynamics

All spacecraft are assumed to be rigid and the reference spacecraft transits in an elliptical orbit. The reference frame, denoted by $\mathcal{F}^r$, has its origin at the centroid of the reference spacecraft. The X_r axis points from the earth center to the reference spacecraft, the Z_r axis is perpendicular to the reference orbit plane, and the Y_r axis can be

obtained according to the right-hand rule. Consider a system with N spacecraft denoted by $\boldsymbol{p}_i = [p_{ix}, p_{iy}, p_{iz}]^\top$, $i = 1, \ldots, N$, and M obstacles in workspace denoted by $\boldsymbol{p}_k^o = \left[p_{kx}^o, p_{ky}^o, p_{kz}^o\right]^\top, k = 1, \ldots, M$. Then, the relative dynamics of spacecraft can be described by (Kristiansen and Nicklasson, 2009)

$$m_i \ddot{\boldsymbol{p}}_i = m_i \boldsymbol{C}_i \dot{\boldsymbol{p}}_i + m_i \boldsymbol{g}_i(\boldsymbol{p}_i) + \boldsymbol{f}_i, \tag{1}$$

where

$$\boldsymbol{C}_i = 2\dot{\theta}_0 \begin{bmatrix} 0 & 1 & 0 \\ -1 & 0 & 0 \\ 0 & 0 & 0 \end{bmatrix},$$

$$\boldsymbol{g}_i(\boldsymbol{p}_i) = \frac{\mu}{r_i^3}\boldsymbol{p}_i - \begin{bmatrix} \dot{\theta}_0^2 & \ddot{\theta}_0 & 0 \\ -\ddot{\theta}_0 & \dot{\theta}_0^2 & 0 \\ 0 & 0 & 0 \end{bmatrix} \boldsymbol{p}_i - \mu \begin{bmatrix} -\frac{r_0}{r_i^3} + \frac{1}{r_0^2} \\ 0 \\ 0 \end{bmatrix},$$

and m_i is the mass of the i-th spacecraft, $\boldsymbol{f}_i$ is the control force vector of the i-th spacecraft, θ_0 is the true anomaly of the reference spacecraft, μ is the gravitational constant of the Earth, r_0 denotes the radial distance of the origin of the reference frame to the Earth's center, $r_i = \sqrt{(r_0 + p_{ix})^2 + p_{iy}^2 + p_{iz}^2}$ is the distance between the Earth's center and the centroid of the i-th spacecraft.

Without special explanation, we use the notation $\boldsymbol{x} = \left[\boldsymbol{x}_1^\top, \ldots, \boldsymbol{x}_N^\top\right]^\top \in \mathbb{R}^{nN}$, where $\boldsymbol{x}_i \in \mathbb{R}^n$. For example, $\boldsymbol{p} = \left[\boldsymbol{p}_1^\top, \ldots, \boldsymbol{p}_N^\top\right]^\top \in \mathbb{R}^{3N}, \dot{\boldsymbol{p}} = \left[\dot{\boldsymbol{p}}_1^\top, \ldots, \dot{\boldsymbol{p}}_N^\top\right]^\top \in \mathbb{R}^{3N}$ and $\boldsymbol{p}^o = \left[\left(\boldsymbol{p}_1^o\right)^\top, \ldots, \left(\boldsymbol{p}_M^o\right)^\top\right]^\top \in \mathbb{R}^{3M}$.

Assumption 1. Since the change of mass m_i of spacecraft is very small, it is assumed that m_i is constant but unknown.

2.2. Algebraic graph theory

The proximity graph between the spacecraft is described by graph theory in this paper. This subsection presents some notions of algebraic graph theory (Mesbahi and Egerstedt, 2010). A weighted graph $\mathcal{G}$ is an ordered triple $(\mathcal{V}, \mathcal{E}, A(\mathcal{G}))$ consisting of a vertex set $\mathcal{V} = \{1, 2, \ldots N\}$, an edge set $\mathcal{E} \subset \mathcal{V} \times \mathcal{V}$, and a weighted adjacency matrix $\boldsymbol{A} = [a_{ij}] \in \mathbb{R}^{N \times N}$. The edge $(i, j) \in \mathcal{E}$ if and only if the vertex j can get information from vertex i, and i is called a neighbor of j. Graph $\mathcal{G}$ is said to be undirected if for any edge $(i, j) \in \mathcal{E}$ means $(j, i) \in \mathcal{E}$. The set of neighbors of the j-th spacecraft is denoted by $\mathcal{N}_j = \{i \in \mathcal{V}(i, j) \in \mathcal{E}\}$. A path of $\mathcal{G}$ is given by a sequence of edges $(i_1, i_2), (i_2, i_3), \ldots$ such that for $k = 1, 2, \ldots$, the edges $(i_k, i_{k+1}) \in \mathcal{E}$. The graph $\mathcal{G}$ is called a connected graph if there is a path for every pair of vertices in $\mathcal{V}$. The adjacency matrix $A(\mathcal{G})$ is defined as: $a_{ij} = 1$ if $(i, j) \in \mathcal{E}(\mathcal{G})$, otherwise $a_{ij} = 0$. Another important matrix of graph $\mathcal{G}$ is the Laplacian matrix $\boldsymbol{L} = [l_{ij}] \in \mathbb{R}^{N \times N}$, which is defined as: if $i = j, l_{ij} = \sum_{j=1}^{N} a_{ij}$, otherwise $l_{ij} = -a_{ij}$.

Lemma 1. *The Laplacian matrix $\boldsymbol{L}$ is symmetric and positive semidefinite if the graph $\mathcal{G}$ is undirected and connected* (Mesbahi and Egerstedt, 2010).

2.3. The dynamic graph model

In this paper, it is assumed that the neighbor relationship between the spacecraft and obstacles are based on their relative distances. Suppose all spacecraft have the same sensing distance Δ. The collision distance between spacecraft i and j is denoted as δ_{ij}. The adjacency matrix $\boldsymbol{A}(\mathcal{G})$ between the spacecraft is generated dynamically according to the current distances as follows:

$$a_{ij}(t) = \begin{cases} 1, & \text{if } ||\boldsymbol{p}_{ij}(t)|| \in \left(\delta_{ij}, \Delta\right), i, j \in \mathcal{V}\}; \\ 0, & \text{otherwise;} \end{cases} \tag{2}$$

where $\boldsymbol{p}_{ij}(t) = \boldsymbol{p}_i(t) - \boldsymbol{p}_j(t), a_{ij} = 1$ indicates spacecraft i can get the states of spacecraft $j, a_{ij} = 0$ otherwise. The definition of adjacency matrix in Eq. (2) indicates that graph $\mathcal{G}$ is undirected.

Suppose the collision distance between spacecraft i and obstacle k is δ_{ik}^o. Then, the adjacency matrix $\boldsymbol{B} = [b_{ik}] \in \mathbb{R}^{N \times M}$ between the spacecraft and the obstacles is defined as

$$b_{ik}(t) = \begin{cases} 1, & \text{if } ||\boldsymbol{p}_{ik}^o(t)|| \in \left(\delta_{ik}^o, \Delta\right), i \in \mathcal{V}, k \in \mathcal{V}^o\}; \\ 0, & \text{otherwise;} \end{cases} \tag{3}$$

where $\boldsymbol{p}_{ik}^o(t) = \boldsymbol{p}_i(t) - \boldsymbol{p}_k^o(t), b_{ik}(t) = 1$ means spacecraft i can sensing obstacle $k, b_{ik}(t) = 0$ otherwise.

Before moving on, we need the following reasonable assumptions.

Assumption 2 (*Initial formation*). Suppose the initial graph $\mathcal{G}(0)$ generated according to Eq. (2) is connected and no collisions have happened at the initial time.

Definition 1 (*Reachable*). The desired configuration $\boldsymbol{p}_d$ is reachable if the following conditions hold (Li et al., 2013)

$$d_{ij} < \Delta, \forall i \in \{1, \ldots, N\}, j \in \mathcal{N}_i,$$

where $d_{ij} = ||\boldsymbol{p}_i^d - \boldsymbol{p}_j^d||$ denotes the desired distance between spacecraft i and j.

Assumption 3 (*Desired formation*). It is assumed that the desired formation $\boldsymbol{p}_d$ is reachable.

Assumption 4 (*Obstacle*). The obstacles only affect the spacecraft in finite time and their velocities are bounded.

3. Control law design

3.1. Artificial potential function

To preserve the connectivity of the communication graph and avoid the collisions between spacecraft and

obstacles simultaneously, the artificial function in this paper is more complicated than traditional artificial potential function. The artificial potential function consists of two parts: the formation potential function $\psi^f(||\boldsymbol{p}_{ij}||)$ and the obstacle avoidance potential function $\psi^o(||\boldsymbol{p}^o_{ik}||)$. The formation potential function $\psi^f(||\boldsymbol{p}_{ij}||)$ is a differentiable nonnegative function of $||\boldsymbol{p}_{ij}||$. It is defined as follows:

$$\psi^f(||\boldsymbol{p}_{ij}||) = \begin{cases} \psi^r(||\boldsymbol{p}_{ij}||), & \text{if } ||\boldsymbol{p}_{ij}(t)|| \in (\delta_{ij}+\epsilon, d_{ij}]; \\ \psi^a(||\boldsymbol{p}_{ij}||), & \text{if } ||\boldsymbol{p}_{ij}(0)|| \in [d_{ij}, \Delta-\epsilon); \\ \psi^d(||\boldsymbol{p}_{ij}||), & \text{if } ||\boldsymbol{p}_{ij}(0)|| \notin [d_{ij}, \Delta-\epsilon) \\ & \text{and} ||\boldsymbol{p}_{ij}(t)|| \in [d_{ij}, \Delta-\epsilon); \\ \psi^d(\Delta-\epsilon), & \text{if } ||\boldsymbol{p}_{ij}(0)|| \in [\Delta, \infty); \end{cases} \tag{4}$$

where $\psi^r(||\boldsymbol{p}_{ij}||)$ is the repulsion function to avoid collisions between the spacecraft, $\psi^a(||\boldsymbol{p}_{ij}||)$ is the attraction function to preserve the connectivity of graph and $\psi^d(||\boldsymbol{p}_{ij}||)$ is the desired formation function to reach the desired configuration. These functions have the following properties:

1. $\psi^f(||\boldsymbol{p}_{ij}||)$ is symmetric and satisfies

$$\nabla_{\boldsymbol{p}_i}\psi^f(||\boldsymbol{p}_{ij}||) = -\nabla_{\boldsymbol{p}_j}\psi^f(||\boldsymbol{p}_{ij}||),$$

   where $\nabla_{\boldsymbol{p}_i}\psi^f(||\boldsymbol{p}_{ij}||)$ denotes the gradient of $\psi^f(||\boldsymbol{p}_{ij}||)$ with respect to $\boldsymbol{p}_i$.
2. $\psi^r(||\boldsymbol{p}_{ij}||)$ is monotonically decreasing with respect to $||\boldsymbol{p}_{ij}||$; $\psi^a(||\boldsymbol{p}_{ij}||)$ and $\psi^d(||\boldsymbol{p}_{ij}||)$ are monotonically increasing with respect to $||\boldsymbol{p}_{ij}||$.
3. All three potential functions attain their unique minimum while $||\boldsymbol{p}_{ij}|| = d_{ij}$ and satisfy the following equation $\psi^r(||d_{ij}||) = \psi^a(||d_{ij}||) = \psi^d(||d_{ij}||)$.
4. $\psi^r(||\boldsymbol{p}_{ij}||) \to \infty$ as $||\boldsymbol{p}_{ij}|| \to \delta_{ij}$, and $\psi^a(||\boldsymbol{p}_{ij}||) \to \infty$ as $||\boldsymbol{p}_{ij}|| \to \Delta$.

According to the repulsion function $\psi^r(||\boldsymbol{p}_{ij}||)$, the obstacle avoidance potential function $\psi^o(||\boldsymbol{p}^o_{ik}||)$ to avoid collisions between the spacecraft and the obstacles can be defined as follows:

$$\psi^o(||\boldsymbol{p}^o_{ik}||) = \begin{cases} \psi^r(||\boldsymbol{p}^o_{ik}||), & \text{if } ||\boldsymbol{p}^o_{ik}(t)|| \in (\delta^o_{ik}+\epsilon, d^o_{ik}]; \\ 0, & \text{if } ||\boldsymbol{p}^o_{ik}(t)|| \in [d^o_{ik}, \infty); \end{cases} \tag{5}$$

where d^o_{ik} denotes the reaction distance between spacecraft i and obstacle k, $d^o_{ik} < \Delta$. From the properties of $\psi^r(||\boldsymbol{p}^o_{ik}||)$, the potential function $\psi^o(||\boldsymbol{p}^o_{ik}||)$ satisfies

1. $\psi^o(||\boldsymbol{p}^o_{ik}||)$ is symmetric and satisfies

$$\nabla_{\boldsymbol{p}_i}\psi^o(||\boldsymbol{p}^o_{ik}||) = -\nabla_{\boldsymbol{p}^o_k}\psi^o(||\boldsymbol{p}^o_{ik}||).$$

2. $\psi^o(||\boldsymbol{p}^o_{ik}||)$ is monotonically decreasing with respect to $||\boldsymbol{p}^o_{ik}||$.
3. $\psi^o(||\boldsymbol{p}^o_{ik}||) \to \infty$ as $||\boldsymbol{p}^o_{ik}|| \to \delta^o_{ik}$ and $\psi^o(||\boldsymbol{p}^o_{ik}||) \to 0$ as $||\boldsymbol{p}^o_{ik}|| \to d^o_{ik}$.

To simplify, the potential functions $\psi^f(||\boldsymbol{p}_{ij}||)$ and $\psi^o(||\boldsymbol{p}^o_{ik}||)$ are abbreviated as ψ^f_{ij} and ψ^o_{ik} in the following part of this paper.

Remark 1. It is important to note that the addition term ϵ in Eqs. (4) and (5) are used to avoid artificial potential function ψ^f_{ij} and ψ^o_{ik} to be infinite. More precisely, it ensures the control inputs will be finite.

Remark 2. It is noted from the definition of ψ^f_{ij} in Eq. 4 that only the initial links of the $\mathcal{G}$ are preserved. However, the new links constructed during formation flying might be broken if these links conflict with other objects, such as collision avoidance with obstacles. This design makes the formation more flexible and can preserve the connectivity of the graph.

3.2. Controller design for static obstacles

In this section, we consider the case while the obstacles are static. The control input for Eq. (1) is specified as

$$\boldsymbol{f}_i = K_c\sum_{j=1}^{N} a_{ij}(t)(\dot{\boldsymbol{p}}_j - \dot{\boldsymbol{p}}_i) - \nabla_{\boldsymbol{p}_i}\Psi + \hat{m}_i\boldsymbol{Y}_i - K_v\dot{\boldsymbol{p}}_i, \tag{6}$$

$$\dot{\hat{m}}_i = -\alpha\dot{\boldsymbol{p}}_i^{\top}\boldsymbol{Y}_i, \tag{7}$$

where $\hat{m}_i$ is the estimation of m_i, α, K_c and K_v are positive constant, Y_i is defined as

$$\boldsymbol{Y}_i = -\boldsymbol{C}_i\dot{\boldsymbol{p}}_i - \boldsymbol{g}_i(\boldsymbol{p}_i), \tag{8}$$

which is independent of m_i, and Ψ is defined as

$$\Psi = K_f\sum_{i=1}^{N}\sum_{j=1}^{N} a_{ij}\psi^f_{ij} + K_o\sum_{i=1}^{N}\sum_{k=1}^{M} b_{ik}\psi^o_{ik}, \tag{9}$$

where K_f and K_o are positive constant.

Theorem 1. *Consider the system of N spacecraft with dynamics Eq. (1) and M static obstacles, with Assumption 1–4 and the designed control law (6 and 7), the desired formation is achieved, the graph $\mathcal{G}(t)$ is connected at all times, and no collisions occur between any spacecraft and obstacles.*

Proof. Consider the following Lyapunov function

$$V_1(t) = \frac{1}{2}\sum_{i=1}^{N} m_i\dot{\boldsymbol{p}}_i^{\top}\dot{\boldsymbol{p}}_i + \frac{1}{2\alpha}\sum_{i=1}^{N}\tilde{m}_i^2 + \Psi, \tag{10}$$

where $\tilde{m}_i = m_i - \hat{m}_i$ denotes the mass estimation error. As $\mathcal{G}(0)$ is connected and no collisions have happened at time t_0. Thus, $V(0)$ in Eq. (10) is finite.

Taking the derivative of Eq. (10) yields

$$\dot{V}_1(t) = \sum_{i=1}^{N} m_i \dot{\boldsymbol{p}}_i^{\top} \ddot{\boldsymbol{p}}_i - \sum_{i=1}^{N} \frac{1}{\alpha} \tilde{m}_i \dot{\hat{m}}_i + \sum_{i=1}^{N} \left(\nabla_{\boldsymbol{p}_i} \Psi\right)^{\top} \dot{\boldsymbol{p}}_i + \sum_{k=1}^{M} \left(\nabla_{\boldsymbol{p}_k^o} \Psi\right)^{\top} \dot{\boldsymbol{p}}_k^o. \tag{11}$$

Using Eq. (1), (6), (7)the fact $\dot{\boldsymbol{p}}_k^o = \boldsymbol{0}$, Eq. (11) can be written as

$$\begin{aligned}
\dot{V}_1(t) &= \sum_{i=1}^{N} \dot{\boldsymbol{p}}_i^{\top} (m_i \boldsymbol{C}_i \dot{\boldsymbol{p}}_i + m_i \boldsymbol{g}_i(\boldsymbol{p}_i) + \boldsymbol{f}_i) - \sum_{i=1}^{N} \frac{1}{\alpha} \tilde{m}_i \dot{\hat{m}}_i \\
&\quad + \sum_{i=1}^{N} \left(\nabla_{\boldsymbol{p}_i} \Psi\right)^{\top} \dot{\boldsymbol{p}}_i \\
&= \sum_{i=1}^{N} \dot{\boldsymbol{p}}_i^{\top} \left(-m_i \boldsymbol{Y}_i + K_c \sum_{j=1}^{N} a_{ij}(t) (\dot{\boldsymbol{p}}_j - \dot{\boldsymbol{p}}_i) - \nabla_{\boldsymbol{p}_i} \Psi + \hat{m}_i \boldsymbol{Y}_i - K_v \dot{\boldsymbol{p}}_i \right) \\
&\quad + \sum_{i=1}^{N} \tilde{m}_i \dot{\boldsymbol{p}}_i^{\top} \boldsymbol{Y}_i + \sum_{i=1}^{N} \left(\nabla_{\boldsymbol{p}_i} \Psi\right)^{\top} \dot{\boldsymbol{p}}_i \\
&= \sum_{i=1}^{N} \dot{\boldsymbol{p}}_i^{\top} \left(K_c \sum_{j=1}^{N} a_{ij}(t) (\dot{\boldsymbol{p}}_j - \dot{\boldsymbol{p}}_i) - \nabla_{\boldsymbol{p}_i} \Psi - K_v \dot{\boldsymbol{p}}_i \right) \\
&\quad + \sum_{i=1}^{N} \left(\nabla_{\boldsymbol{p}_i} \Psi\right)^{\top} \dot{\boldsymbol{p}}_i \\
&= K_c \sum_{i=1}^{N} \sum_{j=1}^{N} a_{ij}(t) \dot{\boldsymbol{p}}_i^{\top} (\dot{\boldsymbol{p}}_j - \dot{\boldsymbol{p}}_i) - K_v \sum_{i=1}^{N} \dot{\boldsymbol{p}}_i^{\top} \dot{\boldsymbol{p}}_i \\
&= -K_c \dot{\boldsymbol{p}}^{\top} [\boldsymbol{L}(t) \otimes \boldsymbol{I}_3] \dot{\boldsymbol{p}} - K_v \dot{\boldsymbol{p}}^{\top} \dot{\boldsymbol{p}},
\end{aligned} \tag{12}$$

where $\dot{\boldsymbol{p}}$ is a column stack vector of $\dot{\boldsymbol{p}}_i, i = 1, \ldots, N$.

Suppose that $\mathcal{G}(t)$ switches at time $t_k (k = 0, 1, \ldots, t_0 = 0)$, otherwise $\mathcal{G}(t)$ is a fixed graph in each time interval $[t_{k-1}, t_k)$. According to Lemma 1, $\boldsymbol{L}(t)$ is positive semi-definite for $t \in [t_0, t_1)$. Thus, $\dot{V}_1(t) \leqslant 0$ and $V_1(t) \leqslant V_1(0)$ for $t \in [t_0, t_1)$. Since the first two items of V_1 are continuous and there are at most $N(N-1)$ links between spacecraft and MN links between the spacecraft and the obstacles. Thus, it is obtained that $V_1(t_1) < \overline{V}_1 = V_1(0) + \Psi_{\max}$, where $\Psi_{\max} = K_f N(N-1)\left[\psi^f(\Delta - \epsilon) + \psi^f\left(\delta_{ij} + \epsilon\right)\right] + K_o MN \psi^o\left(\delta_{ij}^o + \epsilon\right)$. From the definition of Ψ, it is concluded that $V_1(t_1)$ is bounded. Similar to the aforementioned analysis, the time derivative of $V_1(t)$ at $t \in [t_{k-1}, t_k)$ satisfies

$$\dot{V}_1(t) = -K_c \dot{\boldsymbol{p}}^{\top} [\boldsymbol{L}(t) \otimes \boldsymbol{I}_3] \dot{\boldsymbol{p}} - K_v \dot{\boldsymbol{p}}^{\top} \dot{\boldsymbol{p}} \leqslant 0, \tag{13}$$

which indicates that

$$V_1(t) \leqslant V_1(t_{k-1}) < \overline{V}_1, \forall t \in [t_{k-1}, t_k], k = 1, 2, \ldots. \tag{14}$$

In conclusion, $\dot{V}_1(t) \leqslant 0$ and $V_1(t)$ is bounded, which further indicates $\dot{\boldsymbol{p}}_i, \tilde{m}_i, \psi_{ij}^f, \psi_{ik}^o$ are bounded. The boundedness of ψ_{ij}^f and ψ_{ik}^o ensures that no collision happens and no edge in the graph $\mathcal{G}(0)$ will be lost. Furthermore, the inequality $\dot{V}_1(t) \leqslant -K_v \dot{\boldsymbol{p}}^{\top} \dot{\boldsymbol{p}} \leqslant 0$ obviously yields that $\dot{\boldsymbol{p}}_i \to 0$ as $t \to \infty$. Therefore, we known that the velocities of the spacecraft asymptotically converge to zero. Note that the boundedness of $\nabla_{\boldsymbol{p}_i} \Psi$ and $\boldsymbol{Y}_i$ implies $\boldsymbol{f}_i$ is bounded, which in turn implies that $\ddot{\boldsymbol{p}}_i$ is bounded. Overall, $\ddot{V}_1$ is bounded according to Eq. (13). Using Barbalat's lemma one has $\lim_{t \to \infty} \dot{V}_1 = 0$. From the definition of V_1, we have $\nabla_{\boldsymbol{p}_i} \Psi \to 0$ as $t \to \infty$. Assumption 4 indicates that $\nabla_{\boldsymbol{p}_i} \Psi_{ij}^o \to 0$ as $t \to \infty$. The properties of artificial potential function ensure that ψ_{ij} attains its unique minimum while $||\boldsymbol{p}_{ij}|| = d_{ij}$. Thus, $\nabla_{\boldsymbol{p}_i} \Psi_{ij}^f \to 0$ as $t \to \infty$, and one can get that $||\boldsymbol{p}_{ij}|| \to d_{ij}$ as $t \to \infty$ for all $(i, j) \in \mathcal{E}$. □

Remark 3. In literature (Ji and Egerstedt, 2007), the control law ensures the distance between any two agents will only decrease. However, this property can not be provided in this paper as the potential function contains the repulsive function as well as the attractive function.

3.3. Controller design for dynamic obstacles

In the previous subsection, the obstacles are assumed to be static. However, this assumption is hard to be satisfied with practical applications. In this subsection, we consider the case where the obstacles are dynamic. The spacecraft can only access the states of an obstacle while the obstacle is within the sensing region of the spacecraft. Defining the following auxiliary variable

$$\boldsymbol{s}_i = \dot{\boldsymbol{p}}_i - \hat{\boldsymbol{v}}_i, \tag{15}$$

where

$$\hat{\boldsymbol{v}}_i = -\nabla_{\boldsymbol{p}_i} \Psi + K_o \sum_{k=1}^{M} b_{ik} \boldsymbol{w}_{ik}, \tag{16}$$

with

$$\boldsymbol{w}_{ik,q} = \begin{cases} \frac{\left(\nabla_{\boldsymbol{p}_i} \psi_{ik}^o\right)_q \dot{\boldsymbol{p}}_{kq}^o}{\left(\nabla_{\boldsymbol{p}_i} \Psi\right)_q}; & \text{if } \left(\nabla_{\boldsymbol{p}_i} \psi_{ik}^o\right)_q \neq 0, \\ 0, & \text{otherwise;} \end{cases} \quad q = x, y, z, \tag{17}$$

where $\left(\nabla_{\boldsymbol{p}_i} \psi_{ik}^o\right)_q$ and $\dot{\boldsymbol{p}}_{kq}^o$ is the component of $\nabla_{\boldsymbol{p}_i} \psi_{ik}^o$ and $\dot{\boldsymbol{p}}_k^o$ in direction q.

Remark 4. It is noted that if the component $\left(\nabla_{\boldsymbol{p}_i} \psi_{ik}^o\right)_q$ equal to zero, the corresponding denominators in $\boldsymbol{w}_{ik,q}$ equal to zero. To prevent this case, the denominators are modified to a small positive constant v if it equal to zero. However, this case rarely happens as $\nabla_{\boldsymbol{p}_i} \Psi$ contains $\nabla_{\boldsymbol{p}_i} \psi^o$ as an item.

Define a low-pass filter (Hu et al., 2015; Gazi, 2005)

$$\lambda \dot{\boldsymbol{h}}_i = -\boldsymbol{h}_i + \hat{\boldsymbol{v}}_i, \tag{18}$$

where λ is a small constant. By choosing appropriate value of λ similar to (Haskara, 1998), we can obtain

$$\boldsymbol{h}_i \approx [\hat{\boldsymbol{v}}_i]_{eq}, \tag{19}$$

where the subscript "eq" represents the equivalent value of $\boldsymbol{w}_i$ Then, one can obtain

$$m_i\left\|\frac{\mathrm{d}}{\mathrm{d}t}\hat{\boldsymbol{v}}_i\right\| = m_i||\dot{\boldsymbol{h}}_i|| \leqslant \gamma_i, \tag{20}$$

where γ_i is a positive constant.

Then, the following distributed control is proposed

$$\boldsymbol{f}_i = -K_c\sum_{j=0}^{N}a_{ij}(\boldsymbol{s}_i-\boldsymbol{s}_j) - K_s\boldsymbol{s}_i - \beta_i\mathrm{sgn}(\boldsymbol{s}_i) - \nabla_{\boldsymbol{p}_i}\Psi + \hat{m}_i\boldsymbol{Y}_i, \tag{21}$$

$$\dot{\hat{m}}_i = -\alpha\boldsymbol{s}_i^{\top}\boldsymbol{Y}_i, \tag{22}$$

where K_c, K_s and β_i are positive constant, $\boldsymbol{Y}_i$ and Ψ are defined as in Subsection 3.2.

Theorem 2. *Consider a system of N spacecraft governed by Eq. (1) and M dynamic obstacles, with Assumption 1–4 and the designed control law 21 and 22, if $\beta_i > \gamma_i$, then the desired formation is achieved, the graph $\mathcal{G}(t)$ is connected for at all times, and no collisions occur between the spacecraft and obstacles.*

Proof. Consider the following Lyapunov function candidate:

$$V_2(t) = \frac{1}{2}\sum_{i=1}^{N}m_i\boldsymbol{s}_i^{\top}\boldsymbol{s}_i + \frac{1}{2\alpha}\sum_{i=1}^{N}\tilde{m}_i^2 + \Psi. \tag{23}$$

Taking the derivative of (23) obtains

$$\dot{V}_2(t) = \sum_{i=1}^{N}\boldsymbol{s}_i^{\top}m_i\dot{\boldsymbol{s}}_i - \frac{1}{\alpha}\sum_{i=1}^{N}\tilde{m}_i\dot{\hat{m}}_i + \sum_{i=1}^{N}(\nabla_{\boldsymbol{p}_i}\Psi)^{\top}\dot{\boldsymbol{p}}_i + \sum_{i=1}^{M}\left(\nabla_{\boldsymbol{p}_k^o}\Psi\right)^{\top}\dot{\boldsymbol{p}}_k^o. \tag{24}$$

Substituting Eqs. (1), (15), (21) and (22), one can obtains

$$\begin{aligned}\dot{V}_2(t) &= \sum_{i=1}^{N}\boldsymbol{s}_i^{\top}\left[m_i\ddot{\boldsymbol{p}}_i - m_i\dot{\hat{\boldsymbol{v}}}_i\right] + \sum_{i=1}^{N}\tilde{m}_i\boldsymbol{s}_i^{\top}\boldsymbol{Y}_i + \sum_{i=1}^{N}(\nabla_{\boldsymbol{p}_i}\Psi)^{\top}[\boldsymbol{s}_i+\hat{\boldsymbol{v}}_i] + \sum_{i=1}^{M}\left(\nabla_{\boldsymbol{p}_k^o}\Psi\right)^{\top}\dot{\boldsymbol{p}}_k^o\\ &= \sum_{i=1}^{N}\boldsymbol{s}_i^{\top}\left[-\tilde{m}_i\boldsymbol{Y}_i - K_c\sum_{j=0}^{N}a_{ij}(\boldsymbol{s}_i-\boldsymbol{s}_j) - K_s\boldsymbol{s}_i - \beta_i\mathrm{sgn}(\boldsymbol{s}_i) - \nabla_{\boldsymbol{p}_i}\Psi - m_i\dot{\hat{\boldsymbol{v}}}_i\right]\\ &\quad + \sum_{i=1}^{N}\tilde{m}_i\boldsymbol{s}_i^{\top}\boldsymbol{Y}_i + \sum_{i=1}^{N}(\nabla_{\boldsymbol{p}_i}\Psi)^{\top}\left[\boldsymbol{s}_i - \nabla_{\boldsymbol{p}_i}\Psi + K_o\sum_{k=1}^{M}b_{ik}\boldsymbol{w}_{ik}\right] + \sum_{i=1}^{M}\left(\nabla_{\boldsymbol{p}_k^o}\Psi\right)^{\top}\dot{\boldsymbol{p}}_k^o\\ &= \sum_{i=1}^{N}\boldsymbol{s}_i^{\top}\left[-K_c\sum_{j=0}^{N}a_{ij}(\boldsymbol{s}_i-\boldsymbol{s}_j) - K_s\boldsymbol{s}_i - \beta_i\mathrm{sgn}(\boldsymbol{s}_i) - m_i\dot{\hat{\boldsymbol{v}}}_i\right]\\ &\quad - \sum_{i=1}^{N}(\nabla_{\boldsymbol{p}_i}\Psi)^{\top}\nabla_{\boldsymbol{p}_i}\Psi + K_o\sum_{i=1}^{N}\sum_{k=1}^{M}b_{ik}(\nabla_{\boldsymbol{p}_i}\Psi)^{\top}\boldsymbol{w}_{ik} + \sum_{i=1}^{M}\left(\nabla_{\boldsymbol{p}_k^o}\Psi\right)^{\top}\dot{\boldsymbol{p}}_k^o.\end{aligned} \tag{25}$$

Pre-multiplying both sides of Eq. (17) by $(\nabla_{\boldsymbol{p}_i}\Psi)^{\top}$, one can obtain

$$(\nabla_{\boldsymbol{p}_i}\Psi)^{\top}\boldsymbol{w}_{ik} = (\nabla_{\boldsymbol{p}_i}\psi_{ik}^o)\dot{\boldsymbol{p}}_k^o = -\left(\nabla_{\boldsymbol{p}_k^o}\psi_{ik}^o\right)\dot{\boldsymbol{p}}_k^o. \tag{26}$$

Then Eq. (25) can be simplified as

$$\begin{aligned}\dot{V}_2(t) = &-\sum_{i=1}^{N}(\nabla_{\boldsymbol{p}_i}\Psi)^{\top}\nabla_{\boldsymbol{p}_i}\Psi - K_c\boldsymbol{s}^{\top}[\boldsymbol{L}(t)\otimes\boldsymbol{I}_3]\boldsymbol{s}\\ &- K_s\boldsymbol{s}^{\top}\boldsymbol{s} - \sum_{i=1}^{N}\boldsymbol{s}_i^{\top}\left[\beta_i\mathrm{sgn}(\boldsymbol{s}_i) + m_i\dot{\hat{\boldsymbol{v}}}_i\right],\end{aligned} \tag{27}$$

where $\boldsymbol{s}$ is a column stack vector of $\boldsymbol{s}_i, i = 1,\ldots,N$. In view of Eq. (20), it follows that

$$\dot{V}_2(t) \leqslant -\sum_{i=1}^{N}(\nabla_{\boldsymbol{p}_i}\Psi)^{\top}\nabla_{\boldsymbol{p}_i}\Psi - K_c\boldsymbol{s}^{\top}[\boldsymbol{L}(t)\otimes\boldsymbol{I}_3]\boldsymbol{s} - K_s\boldsymbol{s}^{\top}\boldsymbol{s}. \tag{28}$$

Similar to the proof of Theorem 1, one can obtain $\dot{V}_2(t) \leqslant 0$ and $V_2(t)$ is bounded. Thus, $\boldsymbol{s}_i, \tilde{m}_i, \psi_{ij}^f, \psi_{ik}^o$ are bounded. Therefore, there is no collision between the spacecraft and the connectivity of graph $\mathcal{G}(0)$ is preserved. Furthermore, the inequality $\dot{V}_2(t) \leqslant -\sum_{i=1}^{N}(\nabla_{\boldsymbol{p}_i}\Psi)^{\top}\nabla_{\boldsymbol{p}_i}\Psi - K_s\boldsymbol{s}^{\top}\boldsymbol{s}$ obviously yields that $\boldsymbol{s}_i \to 0, \nabla_{\boldsymbol{p}_i}\Psi \to 0$ as $t \to \infty$. Note that $\dot{\boldsymbol{p}}_i = \boldsymbol{s}_i - \nabla_{\boldsymbol{p}_i}\Psi + K_o\sum_{k=1}^{M}b_{ik}\boldsymbol{w}_{ik}$. With Assumption 4, $K_o\sum_{k=1}^{M}b_{ik}\boldsymbol{w}_{ik} = 0$ as $t \to \infty$. Overall, $\dot{\boldsymbol{p}}_i \to 0$ as $t \to \infty$, i.e., the velocities of all spacecraft converge to zero. The fact $\nabla_{\boldsymbol{p}_i}\Psi \to 0$ and Assumption 4 indicate that $\nabla_{\boldsymbol{p}_i}\Psi_{ij}^f \to 0$ as $t \to \infty$. Combining with the properties of artificial function, the desired formation is achieved, i.e., $||\boldsymbol{p}_{ij}|| \to d_{ij}$ as $t \to \infty$ for all $(i,j) \in \mathcal{E}$. □

Remark 5. When the obstacles are dynamic, the controller design in Eq. (21) must involve the velocities of the obstacles, which cannot be eliminated directly. By introducing the velocity terms of the obstacles in the design of sliding manifolds in Eq. (15), the velocity items are canceled out in Eq. (25). Thus, the stability of the closed-loop system can be guaranteed.

4. Simulations

In this section, the comparisons between the proposed controller and a controller without considering connectivity preservation are presented in numerical simulations to demonstrate the effectiveness and superiority of the proposed adaptive control method. In the simulations, the potential function is chosen as:

$$\begin{aligned}\psi_{ij}^r = &\ k_r\left[(\|\boldsymbol{p}_{ij}\| - \delta_{ij}) - d_{ij}\ln(\|\boldsymbol{p}_{ij}\| - \delta_{ij}) + d_{ij}\ln(d_{ij}-\delta_{ij}) - (d_{ij}-\delta_{ij})\right];\\ \psi_{ij}^a = &\ k_a\left[(\Delta - \|\boldsymbol{p}_{ij}\|) - d_{ij}\ln(\Delta - \|\boldsymbol{p}_{ij}\|) + d_{ij}\ln(\Delta - d_{ij}) - (\Delta - d_{ij})\right];\\ \psi_{ij}^d = &\ k_d - k_d\cos\left[\pi(\|p_{ij}\| - d_{ij})/(\Delta - d_{ij})\right].\end{aligned} \tag{29}$$

Their derivatives are

$$\begin{aligned}
\nabla_{\boldsymbol{p}_i}\psi_{ij}^{r} &= k_r\frac{(\|\boldsymbol{p}_{ij}\|-d_{ij})(\boldsymbol{p}_i-\boldsymbol{p}_j)}{\|\boldsymbol{p}_{ij}\|(\|\boldsymbol{p}_{ij}\|-\delta_{ij})};\\
\nabla_{\boldsymbol{p}_i}\psi_{ij}^{a} &= k_a\frac{(\|\boldsymbol{p}_{ij}\|-d_{ij})(\boldsymbol{p}_i-\boldsymbol{p}_j)}{\|\boldsymbol{p}_{ij}\|(\Delta-\|\boldsymbol{p}_{ij}\|)};\\
\nabla_{\boldsymbol{p}_i}\psi_{ij}^{d} &= k_d\pi\sin\left[\frac{\pi(\|\boldsymbol{p}_{ij}\|-d_{ij})}{(\Delta-d_{ij})}\right]\frac{(\boldsymbol{p}_i-\boldsymbol{p}_j)}{\|\boldsymbol{p}_{ij}\|(\Delta-d_{ij})}.
\end{aligned}\tag{30}$$

It is easy to verify that the above functions satisfy the properties of potential functions.

The parameters of the reference orbit are provided in Table 1. It is assumed that all components of a spacecraft or an obstacle can be wrapped by a sphere whose radius is 5 m. In this case, one can easily choose $\delta_{ij}=10$ m and $\delta_{ik}^{o}=10$ m to satisfy the anti-collision requirement. The reaction distance d_{ik}^{o} between spacecraft i and obstacle j is given as 40 m. In addition, supposing the sensing radius of all spacecraft is $\Delta=120$ m. The masses of the spacecraft are $m_1=10$ kg, $m_2=11$ kg, $m_3=11.5$ kg, and the initial masses estimation are set as $\hat{m}_1=\hat{m}_2=\hat{m}_3=10.5$ kg. The initial parameters of the spacecraft and the obstacle are given in Table 2. From the table, it is easy to verify that the initial configuration satisfies Assumptions 2–4. It is assumed that the output forces are thrusters, and the maximum output force component described in the body reference is limited as 1 N.

Table 1
Parameters for the reference orbit.

Orbital parameters	Value
Eccentricity	0.02
Inclination	30°
Longitude ascending node	45°
Semi-major axis	6971 km
Argument of perigee	30°
Initial true anomaly	0°
Gravitational constant	$3.986\times10^{14}(\mathrm{m}^3/\mathrm{s}^2)$

Table 2
Initial parameters of the spacecraft and obstacle

Parameters	Value	Parameters	Value
$\boldsymbol{p}_1(0)$	$[50,70,0]^\top$ m	$\boldsymbol{p}_1^o(0)$	$[60,0,0]^\top$ m
$\boldsymbol{p}_2(0)$	$[0,0,0]^\top$ m	d_{12}	60 m
$\boldsymbol{p}_3(0)$	$[50,-70,0]^\top$ m	d_{23}	80 m
$\dot{\boldsymbol{p}}_i(0)$	$[2,0,0]^\top$(m/s)	d_{13}	100 m

The proposed methods are included in Eqs. (6), (7), (9), (21), (22), (29) and (30), and the corresponding controller taken from (Hu et al., 2015) is listed as follows

$$\begin{aligned}
\boldsymbol{f}_i &= -\gamma\mathrm{sgn}(\boldsymbol{s}_i)-\hat{m}_i\boldsymbol{F}_i-K_d\boldsymbol{s}_i,\\
\dot{\hat{m}}_i &= \alpha\boldsymbol{s}_i^T\boldsymbol{F}_i,
\end{aligned}\tag{31}$$

where

$$\begin{aligned}
\boldsymbol{F}_i &= \tfrac{1}{m_i}(\boldsymbol{D}_i\boldsymbol{p}_i+\boldsymbol{C}_i\boldsymbol{v}_i),\\
\boldsymbol{s}_i &= \dot{\boldsymbol{p}}_i+\tau\nabla_{\boldsymbol{p}_i}J,\\
J &= K_F\sum_{i=1}^{n-1}\sum_{j>i}^{n}J_{ij}(\|\boldsymbol{p}_i-\boldsymbol{p}_j\|)+K_O\sum_{i=1}^{n}J_{io}(\|\boldsymbol{p}_i-\boldsymbol{p}_o\|).
\end{aligned}\tag{32}$$

In the first case, spacecraft formation in the presence of a static obstacle is simulated. Therefore, the velocity of the obstacle is zero. The parameters in Eqs. (6) and (7) are chosen as $K_f=10, K_o=10, K_c=0.1, K_v=0.1$, $k_r=0.2$, $k_a=0.05, k_d=0.2, \alpha=0.01$. The parameters in Eqs. (31) and (32) are set as $K_F=40, K_O=40, K_d=0.1, \alpha=0.5$, $\gamma=0.2, \tau=0.1$.

Fig. 1 shows the distances between the spacecraft in formation, where both controllers ensure the spacecraft reach their desired distances. The red line represents the sensing distance Δ and the blank line represents the collision distance δ. The relative distances between any two spacecraft in the formation are never less than 10 m, so that there is no collision. As seen in the black boxes of Figs. 1a and b, the distances $||\boldsymbol{p}_{12}||$ and $||\boldsymbol{p}_{23}||$ are always less than the sensing distance in 1b, whereas the distances in 1a exceed the sensing distance. This situation implies the communication graph in 1b is disconnected, which results in the formation task can not be completed. For comparison, the connectivity of graph in Fig. 1a is preserved and all space-

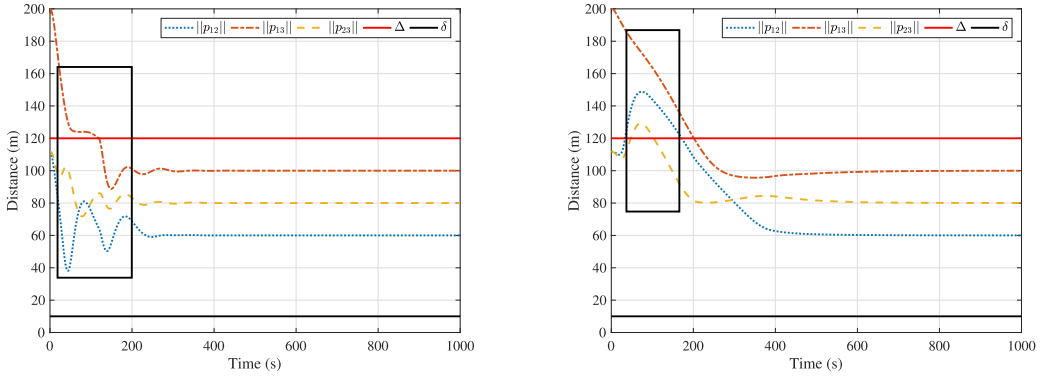

(a) The proposed control law. (b) The control law in (Hu et al., 2015).

Fig. 1. The distances between the spacecraft.

craft can communicate with each other through this connected graph. Figs. 2 and b show the distance between all spacecraft and obstacle 1. Figs. 3 and 4 show the velocities and control inputs of spacecraft with respect to time.

In this second case, spacecraft formation in the presence of a dynamic obstacle is simulated. The obstacle is assumed to carry out a circle with velocity $\dot{\boldsymbol{p}}_1^o = [2\cos(0.01t), -2\sin(0.01t), 0]^\top (\mathrm{m/s})$. The parameters Eqs. (21) and (22) are chosen as $K_f = 50, K_o = 50, K_c = 0.1, K_v = 0.1, k_r = 0.2, k_a = 0.05, k_d = 0.05, \alpha = 0.01, \beta_i = 0.01, \lambda = 0.1$. The parameters in (31) and (32) are set as $K_F = 40, K_O = 20, K_d = 0.1, \alpha = 0.5, \gamma = 0.2, \tau = 0.1$.

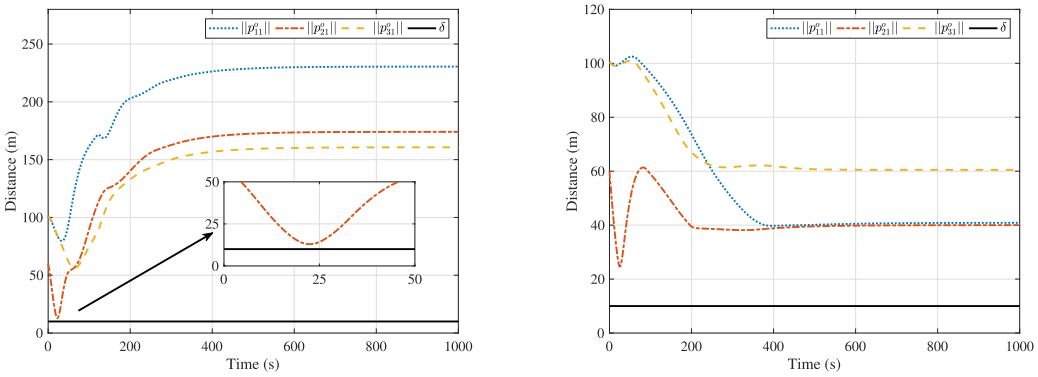

(a) The proposed control law. (b) The control law in (Hu et al., 2015).

Fig. 2. The distances between the spacecraft and the obstacle.

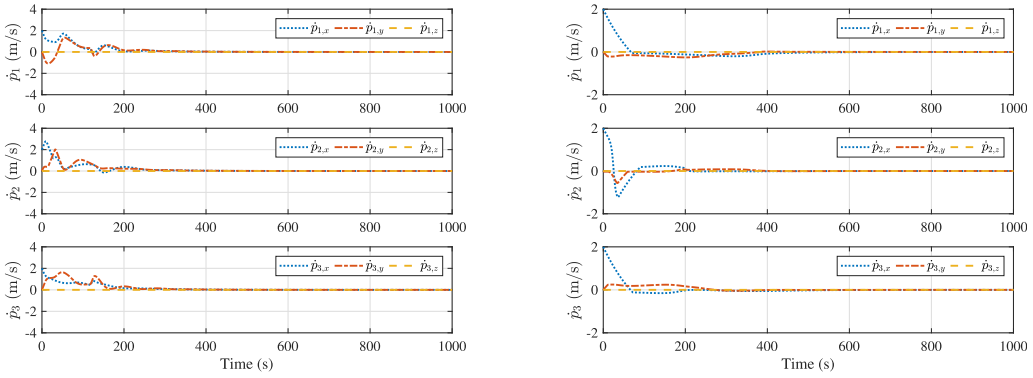

(a) The proposed control law. (b) The control law in (Hu et al., 2015).

Fig. 3. The velocity of the spacecraft.

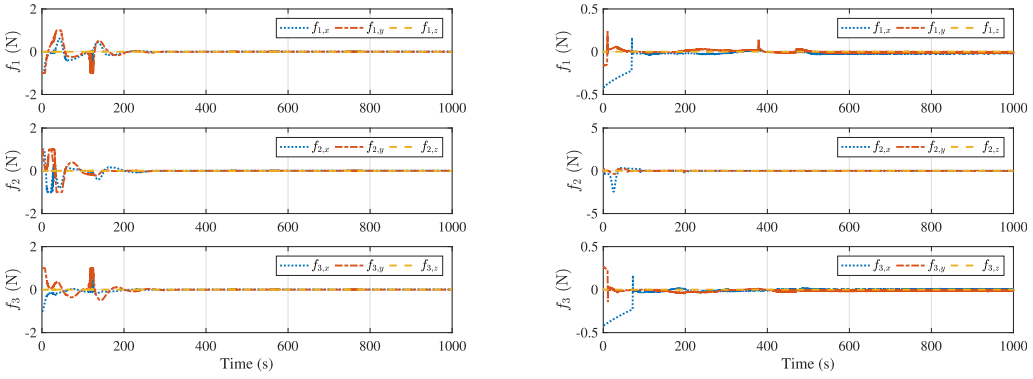

(a) The proposed control law. (b) The control law in (Hu et al., 2015).

Fig. 4. The control inputs.

Fig. 5 show the distances between the spacecraft while Fig. 6 show the distance between the spacecraft and the obstacle. As seen in the figures, the desired formation are achieved and there is no collisions. However, the connectivity of graph in 5a is preserved and that in 5b is not preserved. Figs. 7 and 8 show the velocities and control inputs of spacecraft with respect to time.

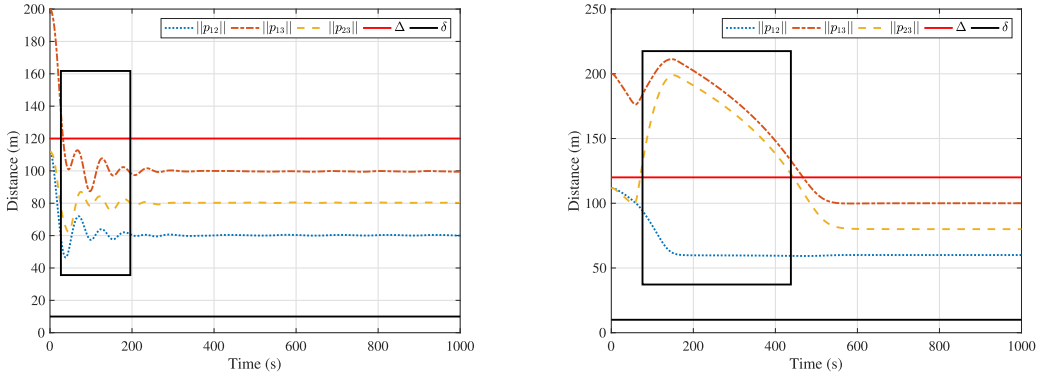

(a) The proposed control law. (b) The control law in (Hu et al., 2015).

Fig. 5. The distances between the spacecraft.

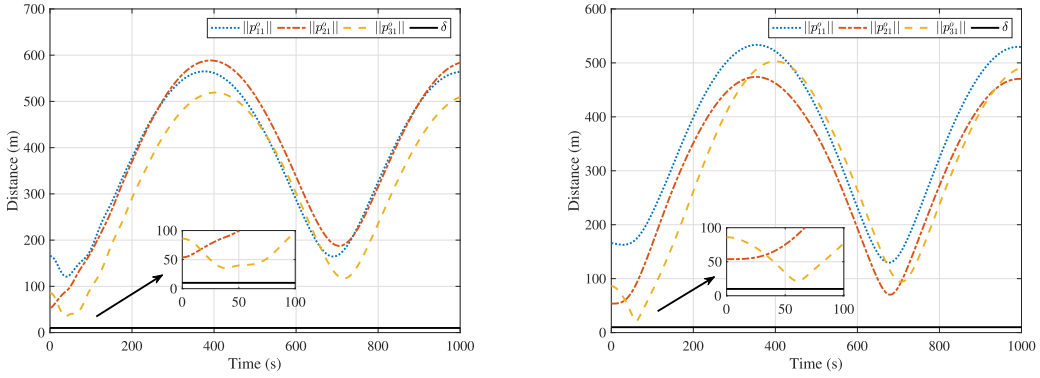

(a) The proposed control law. (b) The control law in (Hu et al., 2015).

Fig. 6. The distances between the spacecraft and the obstacle.

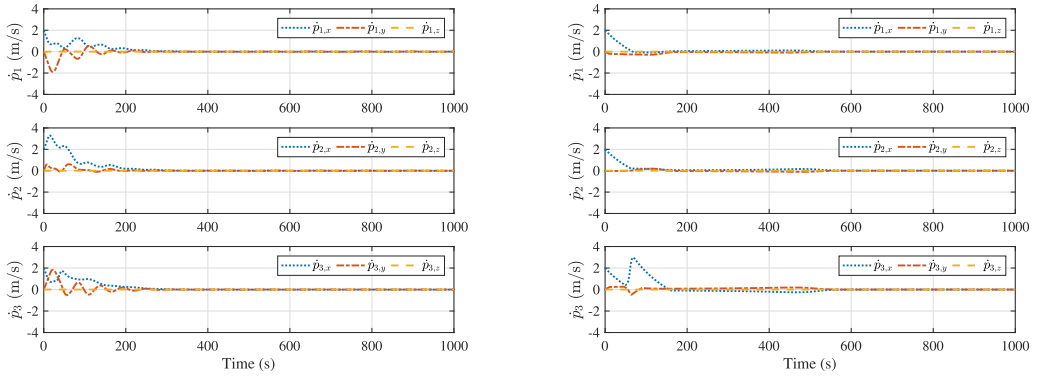

(a) The proposed control law. (b) The control law in (Hu et al., 2015).

Fig. 7. The velocity of the spacecraft.

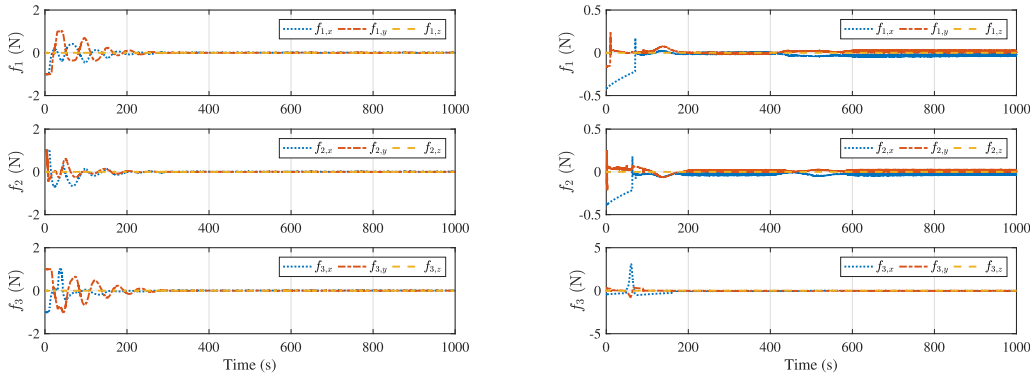

(a) The proposed control law.

(b) The control law in (Hu et al., 2015).

Fig. 8. The control inputs.

5. Conclusions

In the paper, two control algorithms based on potential functions and sliding manifolds are proposed to preserve the connectivity of the communication network and avoid the collisions for spacecraft formation flying in the presence of multiple obstacles. Compared with the current results, our methods do not need the assumption of connectivity of the graph during the SFF. The proposed control laws can automatically guarantee the connectivity at all times if the graph is initially connected. Moreover, the proposed control algorithms require only one-hop neighbors information to achieve connectivity preservation, collision avoidance, desired formation, and velocity matching with each other. Numerical simulations have also been presented to illustrate the theoretical results.

References

Balch, T., Arkin, R.C., 1998. Behavior-based formation control for multirobot teams. IEEE Trans. Robot. Automat. 14 (6), 926–939.

Bandyopadhyay, S., Foust, R., Subramanian, G.P., Chung, S.-J., Hadaegh, F.Y., 2016. Review of formation flying and constellation missions using nanosatellites. J. Spacecraft Rock. 53 (3), 567–578.

Cao, Y., Ren, W., 2012. Distributed coordinated tracking with reduced interaction via a variable structure approach. IEEE Trans. Autom. Control 57 (1), 33–48.

De Gennaro, M.C., Jadbabaie, A., 2006. Decentralized control of connectivity for multi-agent systems. In: Proceedings of the 45th IEEE Conference on Decision and Control. IEEE, pp. 3628–3633.

Deng, J., Wang, L., Liu, Z., Hu, X., 2018. Coordination of multiple rigid bodies under distance-induced interaction topologies. IET Control Theory Appl. 12 (15), 2067–2075.

Di Mauro, G., Lawn, M., Bevilacqua, R., 2017. Survey on guidance navigation and control requirements for spacecraft formation-flying missions. J. Guid. Control Dyn. 41 (3), 581–602.

Dong, Y., Huang, J., 2017. Leader-following consensus with connectivity preservation of uncertain euler–lagrange multi-agent systems. Int. J. Robust Nonlinear Control 27 (18), 4772–4787.

Gasparri, A., Sabattini, L., Ulivi, G., 2017. Bounded control law for global connectivity maintenance in cooperative multirobot systems. IEEE Trans. Rob. 33 (3), 700–717.

Gazi, V., 2005. Swarm aggregations using artificial potentials and sliding-mode control. IEEE Trans. Rob. 21 (6), 1208–1214.

Ghapani, S., Mei, J., Ren, W., Song, Y., 2016. Fully distributed flocking with a moving leader for lagrange networks with parametric uncertainties. Automatica 67, 67–76.

Haskara, I., 1998. On sliding mode observers via equivalent control approach. Int. J. Control 71 (6), 1051–1067.

Hu, Q., Dong, H., Zhang, Y., Ma, G., 2015. Tracking control of spacecraft formation flying with collision avoidance. Aerosp. Sci. Technol. 42, 353–364.

Huang, X., Yan, Y., Zhou, Y., 2017. Underactuated spacecraft formation reconfiguration with collision avoidance. Acta Astronaut. 131, 166–181.

Ji, M., Egerstedt, M., 2007. Distributed coordination control of multiagent systems while preserving connectedness. IEEE Trans. Rob. 23 (4), 693–703.

Kim, Y., Mesbahi, M., 2006. On maximizing the second smallest eigenvalue of a state-dependent graph Laplacian. IEEE Trans. Autom. Control 51 (1), 116–120.

Knorn, S., Chen, Z., Middleton, R.H., 2016. Overview: Collective control of multiagent systems. IEEE Trans. Control Network Syst. 3 (4), 334–347.

Kristiansen, R., Nicklasson, P.J., 2009. Spacecraft formation flying: a review and new results on state feedback control. Acta Astronaut. 65, 1537–1552.

Li, X., Sun, D., Yang, J., 2013. A bounded controller for multirobot navigation while maintaining network connectivity in the presence of obstacles. Automatica 49 (1), 285–292.

Liu, G., Zhang, S., 2018. A survey on formation control of small satellites. Proc. IEEE 106 (3), 440–457.

Lu, M., 2018. Rendezvous with connectivity preservation of mobile agents subject to uniform time-delays. Automatica 88, 31–37.

Mesbahi, M., Egerstedt, M., 2010. Graph Theoretic Methods in Multiagent Networks. Princeton University Press, Princeton.

Qu, Z., Li, C., Lewis, F., 2014. Cooperative control with distributed gain adaptation and connectivity estimation for directed networks. Int. J. Robust Nonlinear Control 24 (3), 450–476.

Sabattini, L., Secchi, C., Chopra, N., 2015. Decentralized estimation and control for preserving the strong connectivity of directed graphs. IEEE Trans. Cybernet. 45 (10), 2273–2286.

Schlanbusch, R., Kristiansen, R., Nicklasson, P.J., 2011. Spacecraft formation reconfiguration with collision avoidance. Automatica 47 (7), 1443–1449.

Stephan, J., Fink, J., Kumar, V., Ribeiro, A., 2017. Concurrent control of mobility and communication in multirobot systems. IEEE Trans. Rob. 33 (5), 1248–1254.

Xue, X., Yue, X., Yuan, J., 2019. Distributed connectivity maintenance and collision avoidance control of spacecraft formation flying. In: 2019 Chinese Control Conference (CCC). IEEE, pp. 8265–8270.

Yue, X., Xue, X., Wen, H., Yuan, J., 2019. Adaptive control for attitude coordination of leader-following rigid spacecraft systems with inertia parameter uncertainties. Chin. J. Aeronaut. 32 (2), 688–700.

Zavlanos, M.M., Egerstedt, M., Pappas, G.J., 2011. Graph-theoretic connectivity control of mobile robot networks. Proc. IEEE 99 (9), 1525–1540.

Zavlanos, M.M., Pappas, G.J., 2007. Potential fields for maintaining connectivity of mobile networks. IEEE Trans. Robot. 23 (4), 812–816.

Zhou, N., Chen, R., Xia, Y., Huang, J., Wen, G., 2018. Neural network–based reconfiguration control for spacecraft formation in obstacle environments. Int. J. Robust Nonlinear Control 28 (6), 2442–2456.

Zou, A., de Ruiter, A.H., Kumar, K.D., 2016. Distributed finite-time velocity-free attitude coordination control for spacecraft formations. Automatica 67, 46–53.